Artificial Organs
31(9):677–688, Blackwell Publishing, Inc.

Flow-induced Platelet Activation and Damage Accumulation in a Mechanical Heart Valve: Numerical Studies

Yared Alemu and Danny Bluestein

Department of Biomedical Engineering, Stony Brook University, Stony Brook, NY, USA

Abstract: A model for platelet activation based on the theory of damage, incorporating cumulative effects of stress history and past damage (senescence) was applied to a three-dimensional (3-D) model of blood flow through a St. Jude Medical (SJM) bileaflet mechanical heart valve (MHV), simulating flow conditions after implantation. The calculations used unsteady Reynolds-averaged Navier–Stokes formulation with non-Newtonian blood properties. The results were used to predict platelet damage from total stress (shear, turbulent, deformation), and incorporate the contribution of repeated passages of the platelets along pertinent trajectories. Trajectories that exposed the platelets to elevated levels of stress around the MHV leaflets and led them to entrapment within the complex 3-D vortical structures in the wake of the valve significantly enhanced platelet activation. This damage accumulation model can be used to quantify the thrombogenic potential of implantable cardiovascular devices, and indicate the problem areas of the device for improving their designs. **Key Words:** Mechanical heart valve—Platelets—Damage—Activation—Blood flow—Numerical methods—Computational fluid dynamics—Thromboembolism.

About 60% of the approximately 120 000 valves implanted each year in the USA are mechanical heart valves (MHVs) (1). Patients with MHV may develop thromboembolic complications (2). Nonphysiologic flow patterns are characterized by elevated shear stresses, with portions of the flow cycle becoming turbulent (3–6). MHVs may induce jet flow, elevated shear stresses, areas of flow separation and recirculation, shed vortices, and turbulence (7).

MHVs are used to restore the function of diseased native valves. During the design evolution of the various MHV models on the market today, valves were optimized mostly with respect to their biocompatibility and hemolytic potential (mechanical damage to red blood cells [RBCs]) (8,9). However, in recent years, it has been recognized that flow-induced thrombogenicity, caused by chronic platelet activation, is the salient aspect of blood trauma in MHV. As MHVs are not necessarily optimized for flow-induced thrombogenicity (9,10), patients receiving even the most updated valves with relatively low thrombogenic potential still require anticoagulant medication due to the risk of thrombogenic complications and cardioembolic stroke.

RBCs have flexible membranes and employ "tank-treading" motion that enables them to sustain much higher stress levels than platelets before they are hemolyzed. Compared to RBCs, platelets have relatively rigid membranes and experience higher membrane strains (11). Hemolysis requires a shear stress of 1500–2500 dyne/cm^2 and exposure time of 102 s (12–14), while platelets will activate at this exposure time at a much lower shear stress of 100–300 dyne/cm^2 (15,16). Measured turbulent stresses in MHV leakage flow (17) indicated that turbulent eddies are in range of platelet activation (18). Platelets are also smaller than the typical Kolmogorov length scale in turbulent energy cascade of MHV flows causing them to respond to viscous shearing (19,20).

Elevated flow stresses and flow patterns that are present in the nonphysiologic geometries of MHV enhance their propensity to initiate thromboembolism. These include adverse pressure gradients, flow

doi:10.1111/j.1525-1594.2007.00446.x

Received August 2006; revised December 2006.
Address correspondence and reprint requests to Dr. Danny Bluestein, Biomedical Engineering Department, Stony Brook University, Stony Brook, NY 11794-8181, USA. E-mail: danny.bluestein@sunysb.edu

separation, and vortex formation that are present in all MHV designs (21). These flow patterns can stimulate the coagulation cascade and initiate thrombosis (17,22,23). Activated platelets with long residence time in these flow regions may aggregate, leading to free emboli formation (23). Exposure to fluid shear stresses will activate and aggregate platelets irreversibly in the absence of any exogenous agonist, showing consistent "dose" and time response characteristics of equivalent chemical agonists (24). Upon activation, platelets change morphology to extend pseudopodia (25), start adhering to surfaces, and aggregate. Aggregation is promoted by agonists secreted from their α-granules (26,27), and by fibrinogen that binds to the platelet surface via GPIIb/IIIa (28). Thrombin is generated when factor Xa is assembled with cofactor Va on the surfaces of activated platelets expressing anionic phospholipids (29). The resulting prothrombinase complex cleaves the soluble fibrinogen into insoluble fibrin—the clot material that may lead to thromboembolic complications.

Experimental measurements in RBC established in the past the relation between shear stress and exposure time, and the hemolysis-induced level of hemoglobin release. Based on these observations, mathematical correlations to estimate the percent hemoglobin release were developed (30,31). A similar model was also developed for platelet activation based on percent release of dehydrogenase (lactate dehydrogenase) from platelets (30). The relation between stress and exposure time that results in hemolysis and in platelet activation has been well established for the case of constant stress. Based on results of numerous researchers, Hellums (32) established a locus of incipient shear-induced platelet activation on a shear stress–exposure time plane, universally referred to as the Hellums' criterion. The threshold for platelet activation according to the Hellums' criterion is represented by a shear stress–exposure time product of 35 dyne·s/cm^2. Although some of the aforementioned models satisfy certain experimental observations, they have also been shown to mostly underestimate cell damage (33,34). Under physiological flow conditions and blood flow through devices, blood is exposed to varying stress levels resulting in blood damage that differs from the ideal case of constant stress (30,34). The magnitude of stress accumulation that leads to cell (RBC/platelet) damage is not clear. For example, in blood flow through devices, the contribution of turbulence to hemolysis and to platelet activation and aggregation may become significant (20). In addition to turbulence, repeated passages through the device expose blood constituents to cyclic loading, which may result in additional cell damage that will precipitate activation (35,36).

Hemolysis response is similar to platelet activation response, and several models for hemolysis have been developed over the years, for example, local rate of hemolysis as a power function of the average local rate of mechanical energy dissipation (37), and relating hemolysis to shear stress (35,36). However, the formulation of an accountable activation/damage accumulation model requires taking into account the dynamic changes characterizing the mechanical loading environment of the platelets in flowing blood within the device, and the cumulative effect of repeated passages past the device (10).

Such an approach was partially developed for modeling hemolysis in devices, assuming that the cell keeps record of past damage (memory) and of the cell age (senescence) such as that the damage (activation or hemolysis) potential is increased (38,39). In these predictive phenomenological models, which are based on the theory of damage in solid mechanics, internal damage accumulates in an RBC until it reaches a critical value of damage, either as a function of the instantaneous stress level and the previous damage history, or as weight average damage accumulation over a number of cycles. While the process of platelet activation is more complex than RBC hemolysis, the conceptual framework is similar. The latter is important for the ability of a model to correspond to the blood flow conditions within the device once implanted in a patient. The blood constituents, and specifically platelets, may be exposed to elevated stresses in their passage through the device, but only intermittently, followed by a refractory period of lower stresses while flowing through the vasculature. With each consecutive passage through the device, the question arises as to what the effect of the previous load history is, or senescence of the platelet, on its activation potential. The current platelet damage accumulation model presented in this article is based on this model.

The current damage accumulation model detailed in this article uses information extracted from the numerical simulation performed to resolve the flow field through the MHV. As such, the ability of the damage model to predict the damage accumulation heavily relies on the quality of the simulation. Recent laminar three-dimensional (3-D) simulations (40–43) depicted the effects of transient flow past MHV and the wake dynamics. However, the laminar flow assumption limits the applicability of these simulations for studying MHV thrombogenicity, as turbulent stresses may easily exceed their laminar counterparts by an order of magnitude, and are critical in activating

the hemostatic system (44). The limitations of most existing turbulence models in handling complex valvular flows (pulsatility entails intermittent turbulence in the transition range, which violates the isotropic turbulence assumption most turbulence models use) restricted the success of their application for solving MHV flows. Kiris et al. (45) solved the steady 3-D Reynolds-averaged Navier–Stokes (RANS) equations in MHV flow, albeit using a simplistic mixing-length turbulence model. Bluestein et al. (3,23) performed unsteady turbulent simulations (unsteady Reynolds-averaged Navier–Stokes [URANS]) using the Wilcox k–ω model (46), which is capable of handling transient turbulence. The k–ω turbulence model was also employed by Yin et al. (47) in comparing the activation potentials of various MHV models (48). The simulations depicted the intricate dynamics of the shed vortices in the wake and quantified stress histories of platelets along pertinent trajectories, with results validated using digital particle image velocimetry (DPIV). Only recently, some more advanced approaches to turbulence modeling in prosthetic heart valves (PHV) flows have been suggested, by using the large eddy simulation approach (49,50).

METHODS

This computational fluid dynamics (CFD) study was conducted to delineate the flow conditions through an MHV implanted in a physiologic geometry, and determine the flow-induced stress accumulation leading to platelet activation damage. Transient and turbulent flow simulations were performed for blood flow in 3-D geometry with a St. Jude Medical (SJM) bileaflet MHV implanted in the aortic position. In this study, blood was considered a two-phase non-Newtonian fluid with spherical solid particles representing platelets. Particle paths calculation took into consideration the influence of the intermittent turbulence present during certain phases of the cardiac cycle. Turbulent and mean flow stress values were extracted for pertinent particle paths. These values were used to calculate platelet stress accumulation and the resulting damage accumulation. Platelet damage accumulation was calculated based on a new damage model that accounts past damage history. The details of the methodology are outlined as follows.

CFD

URANS formulation was applied to solve blood flow through physiologic geometry of bileaflet SJM MHV implanted in the aortic position (Fig. 1). The physiological conditions after MHV implantation were mimicked; the natural geometry of the aortic sinuses was modified to conform with aortotomy (native valve excision). This geometry was based on the *Atlas of Cardiothoracic Surgery* (51), Chaux and Blanche (52), and a previous numerical study by our group (23).

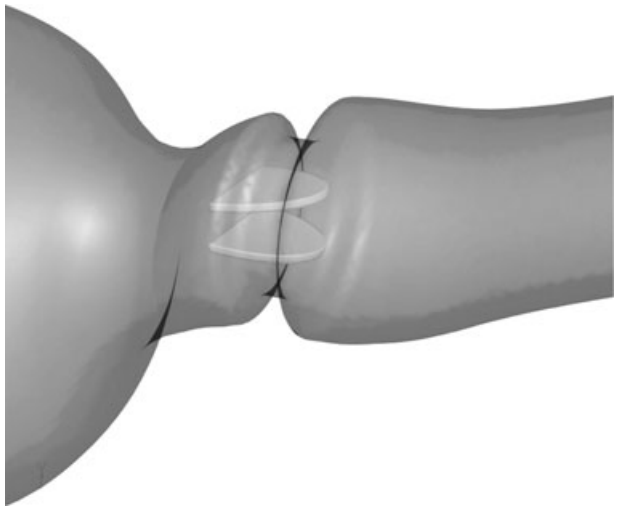

FIG. 1. Investigated valve geometry.

The valve model was tilted 15 degrees from the main flow axis to represent typical misalignment present during implantation. The model has three mesh blocks consisting of tetrahedron, prism, and brick cells, with 670 699 cells total. Progressive density mesh was used to resolve boundary layer flow near all solid boundaries as required by the turbulence model. Model geometry and mesh were constructed using GAMBIT and TGrid with FLUENT solver, finite volume-based CFD package (Fluent, Inc., Lebanon, NH, USA).

In MHV flow, intermittent transient turbulence is present, requiring the use of specialized turbulent models. The Wilcox k–ω turbulence model was chosen for its ability to handle turbulent flow in the transition range (46). The common symmetry assumption applied in numerous MHV simulations to save computational costs has been demonstrated to be inadequate for turbulent simulations (49). The nature of turbulent flow violates imposed geometric symmetry, thus its effect on platelets requires employing a full 3-D geometry even if a symmetry plane is present. Accordingly, a full 3-D geometry was constructed with a simplified leaflet hinge region to facilitate meshing.

The minimal mesh density in the near wall region was dictated by the need in the k–ω model of the first grid point away from the walls to be $y^+ \leq 1$ (y^+, nondimensional viscous sublayer height). The height of Δ, the first grid point from the wall, was computed

according to: $\omega = \frac{6\nu}{c_2\Delta^2}$ (46). With inlet Re = 7300, assuming 10% turbulence intensity (a typical value measured in a pulse duplicator system that was also applied as an initial condition at the inlet), put Δ at a characteristic value of 100 μm, which was used to establish the minimal mesh density in the near-wall region.

Blood was assumed to be two-phase non-Newtonian fluid consisting of fluid carrier phase and neutrally buoyant solid particles representing blood platelets. Two-phase formulation of URANS, which takes into account the particle-fluid interaction, was used to simulate blood flow thorough MHV. Particles used to simulate platelets were seeded at peak systole upstream of the leaflets. Two-phase Lagrangian simulation included about 5000 particles seeded in pertinent regions. The seeding area is about 200 mm^2, which gives a platelet concentration of 25 platelets/mm^2 based on the seeding area.

The simulation was carried out on cardiac velocity waveform used in previous work from our group (23), during deceleration phase up to 300 ms from peak systole before leaflet closure. This corresponds to the phase of the cardiac cycle in which the elevated turbulent stresses and the shed vortices formed in the valve's wake contribute to platelet activation and aggregation. Under pulsatile flow conditions, the turbulence is intermittent, peaking only during the deceleration phase following peak systole (53,54).

The simulation consisted of 3000 time steps with a uniform step size of 1×10^{-4} s. Turbulent particle paths were computed using the stochastic model developed by Gosman and Ioannides (55), in which the instantaneous velocities in the carrier phase are used to solve the particle velocities by adding random fluctuations obtained from the turbulent Wilcox *k*–ω simulation.

Under low levels of shear such as pertain to recirculation regions and vortices populating the valve's wake, the blood non-Newtonian viscosity characteristics overwhelm its Newtonian characteristics. Accordingly, the blood was modeled as a non-Newtonian viscoelastic fluid, with density of ρ = 1.056 g/cm^3 and yield shear of 0.1/s. The shear dependent viscosity was extracted by curve fitting experimental data of human blood viscosity (μ) at 37°C and changing shear rates ($\partial U/\partial y$) (56) according to

$$\mu = A\left(\frac{\partial U}{\partial y}\right)^{(B-1)} + C,$$

$A = 2.6314 \times 10^{-2}$, $B = 0.47234$, $C = 3.117316 \times 10^{-3}$, approximating μ = 3.5 cPoise at elevated shear levels ($\partial U/\partial y > 100$/s).

Unlike laminar flow conditions, in which the computation of platelet activation by stress accumulation requires only the knowledge of the laminar shear stresses, under turbulent flow conditions all components of the stress (mean and turbulent Reynolds stresses) need to be taken into account. The Reynolds stress components were extracted from the total stress tensor by applying the Boussinesq approximation as outlined below.

The total stress tensor includes both the mean and the turbulent stress components:

$$\bar{\tau}_{ij} = \mu\left(\frac{\partial u_i}{\partial x_j} + \frac{\partial u_j}{\partial x_i}\right) - \rho\overline{u_i' u_j'} \tag{1}$$

where $\bar{\tau}_{ij}$ is the stress sensor, μ is the viscosity, $\frac{\partial u_i}{\partial x_j}$ is the mean velocity gradient, ρ is the density, and $\overline{u_i' u_j'}$ is the turbulent/Reynolds stress.

Boussinesq approximation was substituted for the Reynolds stress component of the total stress tensor accordingly:

$$\bar{\tau}_{ij} \approx \mu\left(\frac{\partial u_i}{\partial x_j} + \frac{\partial u_j}{\partial x_i}\right) + \frac{2}{3}\rho k\delta_{ij} - \mu^t\left(\frac{\partial u_i}{\partial x_j} + \frac{\partial u_j}{\partial x_i}\right) \tag{2}$$

where *k* is the turbulent kinetic energy, and μ^t is the turbulent viscosity.

The following two components of the tensor are given to show the general form of all tensor components:

$$\begin{aligned}\bar{\tau}_{11} &\approx \mu\left(\frac{\partial u_1}{\partial x_1} + \frac{\partial u_1}{\partial x_1}\right) + \frac{2}{3}\rho k - \mu^t\left(\frac{\partial u_1}{\partial x_1} + \frac{\partial u_1}{\partial x_1}\right) \\ &= 2\mu\left(\frac{\partial u_1}{\partial x_1}\right) + \frac{2}{3}\rho k - 2\mu^t\left(\frac{\partial u_1}{\partial x_1}\right)\end{aligned} \tag{3}$$

$$\bar{\tau}_{12} \approx \mu\left(\frac{\partial u_1}{\partial x_2} + \frac{\partial u_2}{\partial x_1}\right) - \mu^t\left(\frac{\partial u_1}{\partial x_2} + \frac{\partial u_2}{\partial x_1}\right) \tag{4}$$

The values of viscosity, turbulent viscosity, turbulent kinetic energy, and components of mean velocity gradient were extracted accordingly for pertinent platelet trajectories in which the stress accumulation was computed. The components of the stress tensor were then rendered into a scalar stress value based on the formulation outlined by Apel et al. (36).

$$\sigma = \frac{1}{\sqrt{3}}\sqrt{\begin{array}{c}\tau_{11}^2 + \tau_{22}^2 + \tau_{33}^2 - \tau_{11}\tau_{22} - \tau_{22}\tau_{33} - \tau_{11}\tau_{33} + \\ 3\left(\tau_{12}^2 + \tau_{23}^2 + \tau_{13}^2\right)\end{array}} \tag{5}$$

where σ is the scalar stress.

The stress accumulation calculation was then performed by a summation of the instantaneous product of this scalar value of the total stress and the exposure time between successive nodal points along the platelet trajectory:

$$\sum \sigma \times \Delta t \tag{6}$$

where Δt is the time step.

The same particle paths that were used in the stress accumulation calculation were then used for the damage accumulation model described as follows.

Damage model

The relation between stress, exposure time, and platelet damage can be described by a damage rate equation (38). Following a mathematical model for hemolysis based on theory of damage, there exists a phenomenological damage index, D (representing platelet activation/damage in this work), which reflects the cumulative damage sustained by the platelets' exposure to varying stress levels. This index takes into account the initial damage accumulation (i.e., senescence, or previous damage history during previous passages through the MHV), the stress loading history, and the dependence on the loading rate. In this formulation, the damage assumes normalized values between 0 (no activation/damage) and 1 (full activation/damage). A possible formulation of this damage accumulation is described by the following transcendental equation (38):

$$\dot{D}(t) = \left(\frac{\sigma}{\sigma_0}\right)^r \frac{1}{[1 - D(t)]^k} \tag{7}$$

While this transcendental equation can be integrated directly to yield $D(t)$, consideration should be given to the damage accumulation curve which requires a positive slope to ensure that cell damage always accumulates. This entails that in the damage rate equation, the first derivative of damage needs to be positive at all times. To achieve this behavior, k is assigned a negative value.

The behavior of the solution for Eq. 8 is depicted in Fig. 2 for an idealized case of linearly increasing damage (D) and stress (σ). From this plot, we can infer the behavior of the damage curve for the case of a nonlinear damage accumulation at various ranges of damage (D), namely that damage accumulation behavior, as observed experimentally in platelets (57,58), includes the following three distinct phases: initial lag phase, constant accumulation phase, and refractory effect of tapering off when approaching full activation.

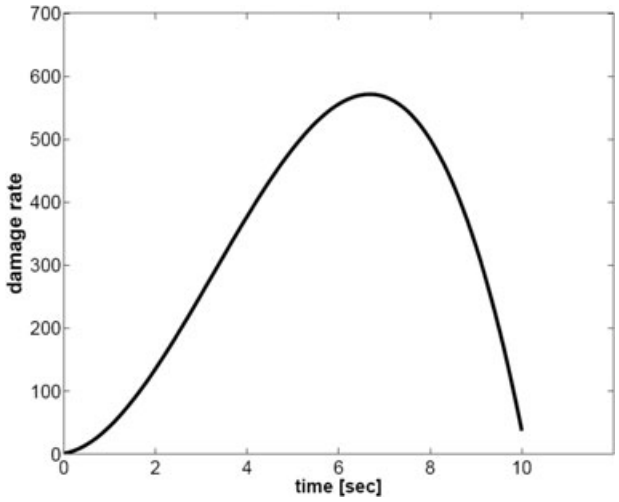

FIG. 2. Behavior of the damage rate according to the damage accumulation equation.

After integrating Eq. 8, an equation for platelet damage accumulation is obtained. In Eq. 9, the initial damage $D(t_0)$ reflects the platelet senescence, or the damage accumulated during previous passages of the platelet through the valve, and can assume a random value between 0 and 1:

$$D(t) = D(t_0) + \int_{t_0}^{t} \left(\frac{\sigma(t)}{\sigma_0}\right)^r \frac{\mathrm{d}t}{[1 - D(t)]^k} \tag{8}$$

The transcendental equation is difficult to integrate without prior knowledge of the stress and damage accumulation behavior. Fortunately, the information (both spatial and temporal) can be extracted from the CFD simulation, along any desired trajectory. For numerical utilization, Eq. 9 is transformed into the following discrete summation form:

$$D(t_i) = D(t_{i-1}) + \left(\frac{\sigma(t_i)}{\sigma_0}\right)^r \frac{\Delta t}{[1 - D(t_{i-1})]^k}, \quad i = 1, 2, \ldots, \max. \tag{9}$$

For ideal cases where the stress is monotonously increasing, decreasing, or is kept constant, the damage accumulation is given in Fig. 3a–c correspondingly, for two assigned initial damage values of 0 and 0.5. The damage accumulation curves are always increasing and the maximum attainable damage value is 1. The k and r values of the damage accumulation function were fixed at −1 and 5, respectively. A negative value of k gives the desired behavior of the damage accumulation curve as observed from the damage rate plot in Fig. 2. The

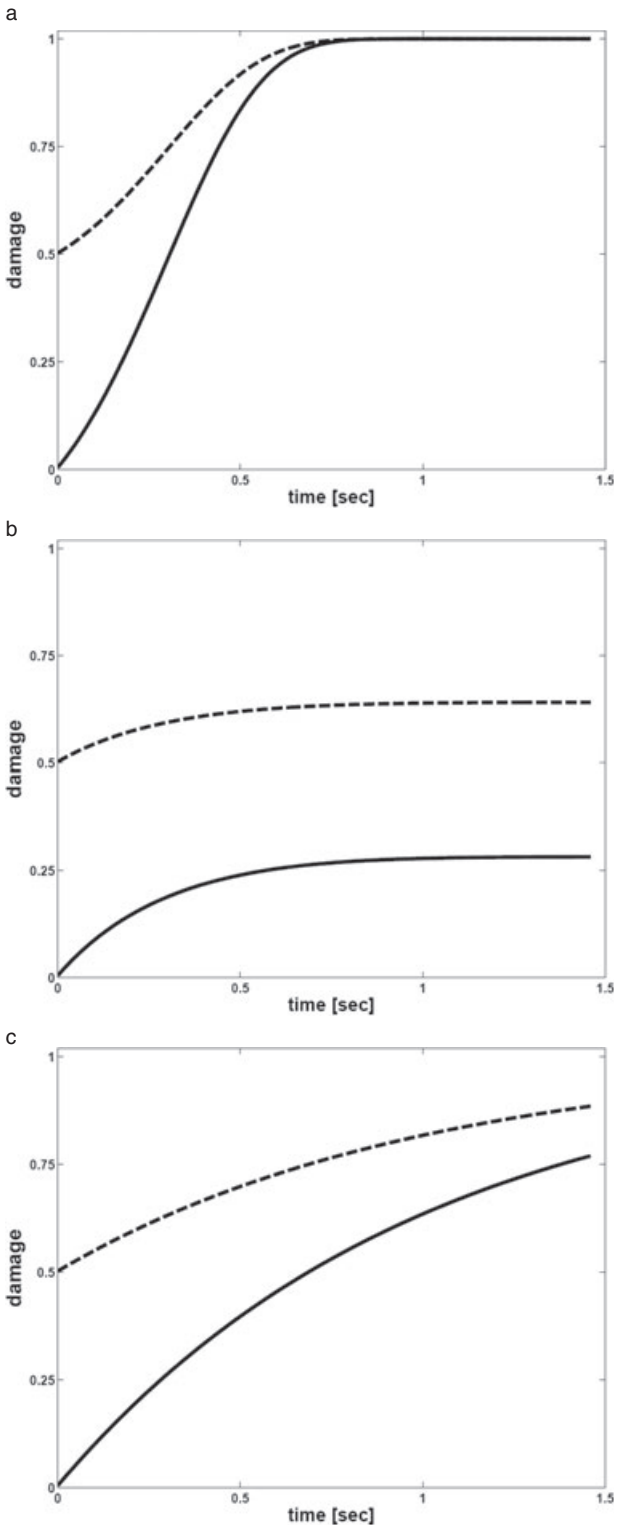

FIG. 3. (a) Damage accumulation behavior for increasing stress. (b) Damage accumulation behavior for decreasing stress. (c) Damage accumulation behavior for constant stress.

sensitivity of the damage accumulation curve to stress is prescribed by the r value, which is increased from unity to produce rapid damage accumulation. The initial damage value, $D(t_0)$ dictates the behavior of the damage accumulation rate as can be observed from the difference in the slopes of the two initial damage cases (0 and 0.5) (Fig. 3a–c). The concavity of the damage accumulation curve is confirmed if the stress is increasing or decreasing over time (38,39), as depicted by the damage accumulation curves (Fig. 3a–c). These curves were specifically generated for ideal cases where the dynamic stress behavior is known a priori (i.e., monotonously increasing, decreasing, or constant over time). These ideal cases were used to establish the validity of the damage accumulation model behavior, before testing it with actual trajectories stress data that dynamically change from one point to the other.

The methodology for computing the damage accumulation curves is as follows: first, the numerical simulation was performed to resolve the flow field through the MHV. Next, the stress accumulation, including Reynolds stresses contribution, was calculated along pertinent trajectories. Finally, damage accumulation was calculated for those trajectories according to Eq. 10. For the damage accumulation calculations, the platelets were assumed to flow repeatedly along the same trajectories during the multiple passages through the valve. The platelets were also assumed to acquire a "perfect memory," that is, for each repeated passage the cumulative damage at the end of that trajectory was applied as the new initial damage value (senescence) for the subsequent passage.

RESULTS

Flow field

The complex, time-dependent 3-D nature of the flow field through MHV makes its presentation challenging. To illustrate the intricate dynamics of the flow field, flow trajectories in the region of the bileaflet MHV lower leaflet are presented in Fig. 3. Particles that were seeded upstream of the lower leaflet emanating from a traverse rack reveal the presence of complex helical vortices from both sides of the leaflet that entrain the fluid toward a central jet that dominates the flow field in the valve's wake (Fig. 4). Additional information about the flow can be obtained from the following cross sections chosen to illustrate some important features of the flow field (Figs. 5–9). The helical vortices generated above the lower leaflet (Fig. 4) counter-rotate and meet on the symmetry midplane. If a longitudinal symmetry cross

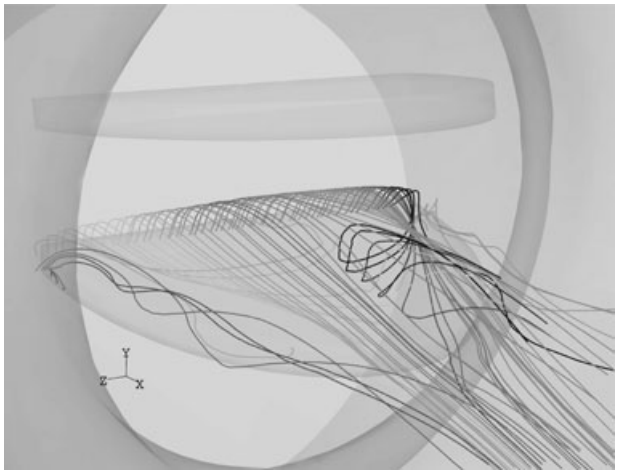

FIG. 4. Smoothed path lines depicting the complex flow dynamics and helical vortices developing in the flow field above the lower leaflet.

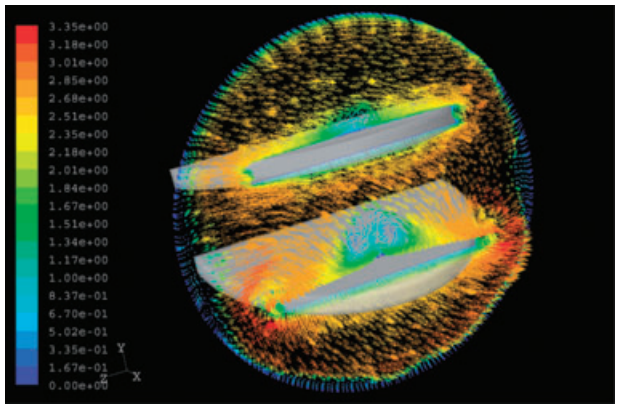

FIG. 7. Velocity vector plot of flow past the valve at peak systole (radial cross section).

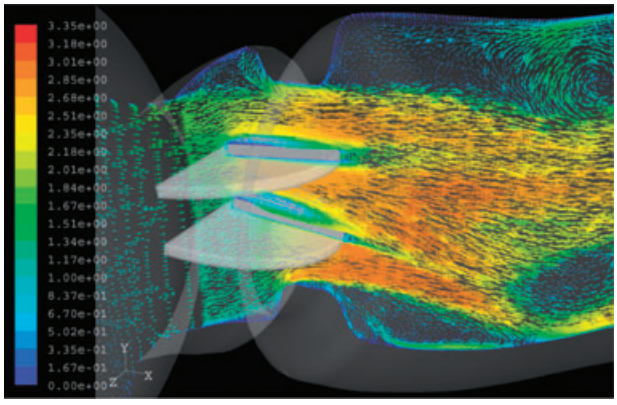

FIG. 5. Velocity vector plot of flow past the valve 30 ms after peak systole (2.5 mm off the midplane cross section).

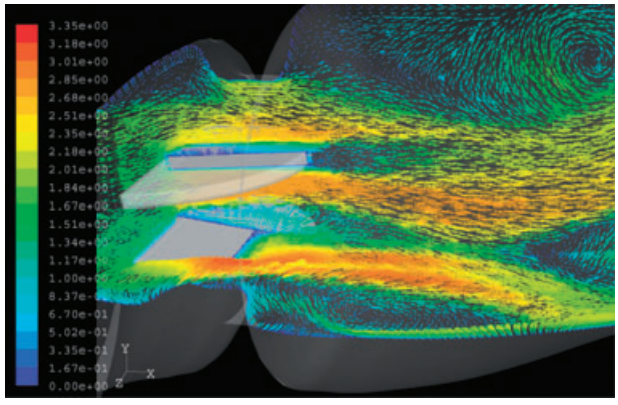

FIG. 8. Velocity vector plot of flow past the valve 30 ms after peak systole (orthogonal cross sections).

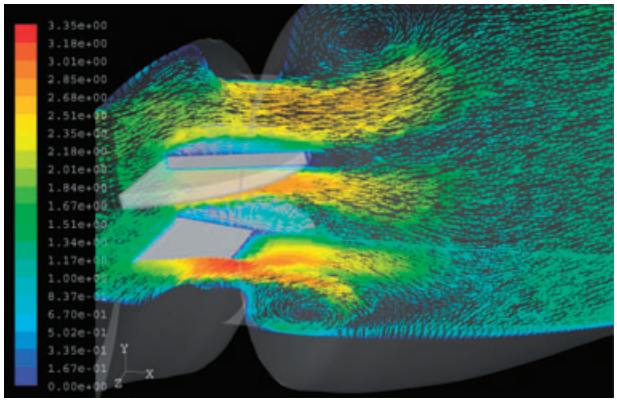

FIG. 6. Velocity vector plot of flow past the valve at peak systole (orthogonal cross sections).

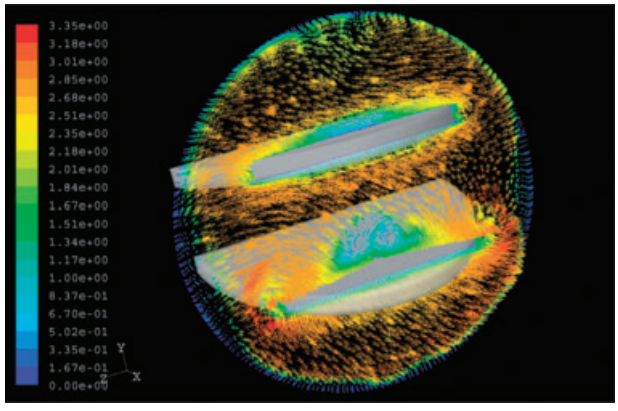

FIG. 9. Velocity vector plot of flow past the valve 30 ms after peak systole (radial cross section).

sectioning is chosen to show the downstream development of the flow field, some important features of the flow field like the prominent flow separation that dominate the flow field above the lower leaflet may be masked. For this reason the cross-sectional plane shown in Fig. 5 is 2.5 mm off the symmetry midplane, depicting this prominent flow separation (30 ms after peak systole). At this time point, the flow separation limits the cross-sectional available for blood flow passage, resulting in three strong jets that dominate the flow field above, in between, and below the leaflets. Strong shear layers are formed between these jets and the recirculating flow in the flow separation zones.

The velocity vector field through the valve is presented in a pair of figures (Figs. 6 and 7 both set at the same phase of the flow cycle, during peak systole). In Fig. 5, two orthogonal cross-sectional planes along the flow direction depict the recirculation zones that are formed in the aortic root sinuses, and regions of flow separation above both leaflets. A larger flow separation region is generated above the lower leaflet. The lateral cross section reveals an area of maximal velocity of about 3.3 m/s generated in the gap region between the edge of the lower leaflet and valve housing. The radial cross section (Fig. 7) depicts the counter-rotating structures of the helical vortices that are formed above the lower leaflet. The next pair of figures (Figs. 8 and 9) employs the same views as those of Figs. 6 and 7 at 30 ms after peak systole. These figures depict the dynamics and the temporal development of the complex flow patterns past the valve during the deceleration from peak systole. The recirculation zones that were generated in the aortic root sinuses expand toward the center of the flow field and extend further downstream, in the process entraining more fluid toward the MHV's wake while strengthening and elongating the central jet through the valve. The radial cross section (Fig. 9) depicts the dynamics of the counter-rotating helical vortices that were present at peak systole, now moving laterally from side to side (these vortex dynamics are best seen with an animation of the transient solution).

Stress and damage accumulation

The two-phase flow calculation of particles representing platelets was used to establish pertinent particle trajectories that pass through the "hot spot" areas in the valve, that is, recirculation zones, the strong jets, and the spiral vortices, and the interfaces between them. Those characteristic trajectories were then used for the stress and damage accumulation calculations. Plots of four representative platelet trajectories and their corresponding stress accumulation are presented (Fig. 10). The figure shows a composite of the selected path lines and their corresponding stress accumulation curves (plotted with the same color). For the selected particle paths, the stress accumulation values range from 8 to 1 dyne·s/cm^2, in the high and low stress regions, respectively. The particle path corresponding to a platelet flowing in the core flow region between the two leaflets (depicted by the solid curve), has a brief residence time, thus lower stress accumulation value. The two particle paths with the highest stress accumulation values (the dashed-dot and dashed-line curves) are trajectories of platelets that were recruited to the helical vortices. The path corresponding to the dotted line curve originated in a shear layer, where it was first exposed to elevated stresses (rapid initial accumulation) then carried away into low stress region, as evident from the low stress accumulation in the second half of the dotted line curve.

From the particle paths used for the stress accumulation calculations described earlier, two representative paths were selected to calculate the amount of platelet damage accumulation and its dependence on the platelet initial damage (senescence) during repeated passages through the valve. The first path is of a platelet in the helical vortex above the lower leaflet typically exposed to elevated stresses and longer exposure time, while the second path is of a platelet flowing in the core region typically exposed to much lower stresses for a shorter duration (the paths corresponding to the solid and dashed lines in Fig. 11, respectively). As outlined in Eq. 10, damage accumulation uses values of stress, exposure time, and the initial damage (the previous damage history)

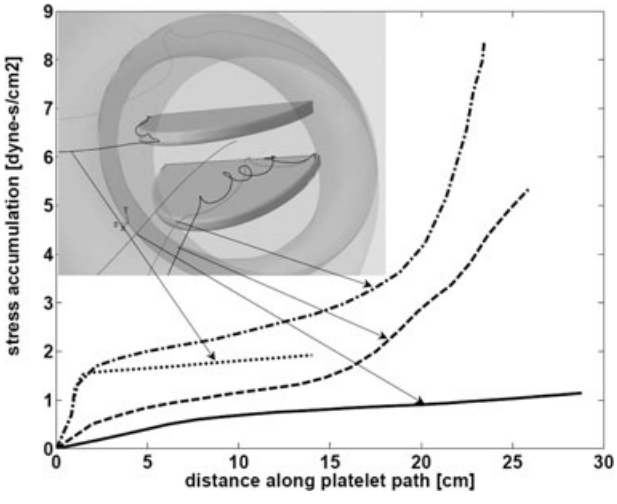

FIG. 10. Stress accumulation (platelet level of activation) with the corresponding platelet trajectories.

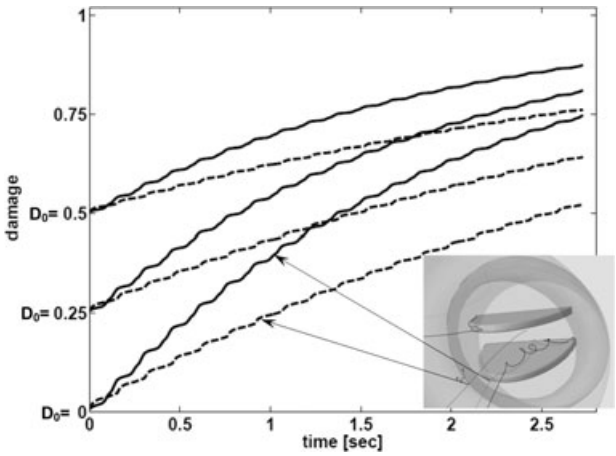

FIG. 11. Damage accumulation during repeated passages past the valve, with the corresponding platelet trajectories.

to obtain the level of cumulative damage in subsequent passages. To assess the damage model behavior, three cases of initial damage values, $D(t_0) = 0$, 0.25, 0.5, were assigned for these platelet trajectories. The damage accumulation plot shows the cumulative damage of platelets that completed 18 repeated passes through the valve region (Fig. 11). This translated into the wiggling behavior noticeable in these accumulation curves. For the case of no initial damage, $D(t_0) = 0$, final damage values of approximately 0.4 and 0.75 were obtained for trajectories through the low and high stress regions, respectively. For higher initial damage values, the damage accumulation rates rather tapered off (more quickly so with higher initial damage value), but the total cumulative damage was higher and was achieved earlier.

DISCUSSION

The implanted MHV geometry used in this study incorporates slight misalignment of the implanted valve geometry. This misalignment establishes a low-pressure region above the leaflet leading to flow separation and formation of counter-rotating spiral vortices between the MHV leaflets which entrain fluid toward the center (40). These flow structures result in decreased flow cross section, strong jets, high velocity gradient, and high shear stress, all of which contribute to platelet stress damage. Spiral vortices draw platelets from the core flow to the high shear regions near the solid boundaries. The interfaces between these strong jets and the recirculation and flow separation zones generate strong shear layers that expose platelets to elevated stresses. The helical vortices then entrain the platelets toward the MHV wake. It reiterates the role of the wake dynamics in activating platelets, and the dominant role in the recruitment and aggregation of platelets that were activated in previous flow phases. It is postulated that these wake dynamics are the origins of cerebrovascular microemboli associated with MHV. They provide the necessary conditions for hemostatic reactions by providing optimal mixing for platelet aggregation, increasing the procoagulant surfaces needed for the coagulation reactions to proceed, and dispersing the clotting factors in the process. Prior activation and the extrusion of platelets pseudopodia, which may be induced by the elevated shear stresses globally preceding vortex dynamics, increase their effective hydrodynamic volume by several folds, resulting in an increased collision rate (59). The ensuing turbulent eddies enhance mixing and cascade energy to ever smaller spatial scales, while dissipating it (the Kolmogorov cascade). When scales are comparable to cellular scales, eddies directly interact with the cells, damaging their membranes (20).

The lateral dynamics of the helical vortices that were observed is characteristic of the inherent unsteadiness of transient turbulence. It invalidates a possible symmetry assumption that may have been used to reduce the size of the numerical mesh by half, and the ensuing computational costs involved. Such an assumption would eliminate these vortex dynamics.

The noticeable strengthening of the jets 30 ms after peak systole, when the main flow field is actually dwindling because of the main flow deceleration, is attributed to the dynamics of the aortic root recirculation zones and their interaction with the central flow in the MHV wake. The elongation and expansion of these recirculation zones toward the center of the flow field limits the cross-sectional area available for the flow passage in the central region, inducing local acceleration that feeds the central jets even though the main flow field is losing energy during deceleration.

A new platelet damage accumulation model relating dynamic varying stress levels (faithfully representing physiologic flow conditions), incorporating the effects of platelet senescence and repeated passages through the valve, was applied to the results of the non-Newtonian URANS simulation of blood flow past the MHV. The complex flow dynamics revealed regions combining elevated stresses with long residence times in the recirculation zones and the helical vortices populating the wake. These resulted in "hot spot" areas in which values of stress accumulation were high. This is clearly seen from the behavior of stress accumulation curves in trajectories

through spiral vortices and core flow region (Fig. 10). The MHV geometry controls the dynamics of the resulting flow structures, which in turn dictates the rate of stress accumulation.

While there are several formulations for platelet activation under the combined effect of stress and exposure time, for example, power law-type relation proposed by others (60), a linear stress–exposure time summation was applied. Notwithstanding, our model involves a summation of the instantaneous product of shear stress and exposure times along the platelet trajectory (successively computed between adjacent numerical nodes). In other words, it is not mere integration of the shear stress over time, as both are independent parameters that continuously change according to the platelet velocity and the shear level encountered along the turbulent platelet trajectory. In this manner, the transient nature of the flow field is incorporated into the model via the continually changing shear–exposure product. The "linear" summation of this instantaneous product is a first approximation of platelet activation under unsteady flow conditions, in the absence of a better, accountable, model for platelet "damage" accumulation. Actual stress accumulation may deviate from the one predicted by linear summation.

As mentioned earlier, the relation between stress accumulation and platelet activation was established experimentally mostly for constant stress loading. The established threshold value for platelet activation under constant shear stress and exposure times (35 dyne·s/cm^2, also known as the Hellums criterion) represents a conservative upper limit, as experimental evidence indicates that under dynamic flow conditions platelets are activated earlier.

The effect of the platelet senescence and the repeated passages through the valve reveals a dynamic response in which the platelet activation rate tapers off as it accumulates damage. This type of refractory effect was observed experimentally both in RBCs and in platelets (57,58), and corresponds to the behavior in the damage accumulation curves (Fig. 11). The level of initial damage, $D(t_0)$, dictates the rate of damage accumulation, with higher initial damage slowing down this rate. However, higher initial damage led to higher total cumulative damage that was achieved earlier, clearly indicating that predictive damage accumulation models should include platelet senescence. During their lifetime, platelets pass through the heart and its valves numerous times. Clearly, flow-induced platelet activation requires multiple passes. The current simulation was restricted to 300 ms of the cardiac cycle (from peak systole until just before leaflet closure), and to 18 passages past the aortic valve. Damage accumulation was calculated assuming the platelets arriving at peak systole and continuing to do so during repeated passes. In the current formulation of the damage accumulation model, platelets were assumed to have "perfect memory" of damage incurred on them during the past passages through the valve. In addition, platelets were assumed to follow the same trajectory during these repeated passages. The results of our model indicate a continually increasing value of damage, demonstrating the cumulative effect that may eventually drive platelets beyond their activation threshold. Under the physiologic scenario, platelets flow through regions of much lower stresses in the vasculature between passages through the valve, and may have mechanisms of damage recovery. Additionally, platelets will not patently flow through the "hot spot" regions of the valve during subsequent passages. Accordingly, actual damage accumulation may be lower than the one predicted by our model. The values of r and k of the damage model (Eq. 10) were assigned based on the conditions set by the damage rate (first derivative) equation. Adjustment of these values based on experimental data will be the focus of future work.

Various activation pathways and feedback loops are involved in platelet activation process, possibly accelerating activation. These are not represented in the model, which corresponds only to the mechanical stimuli. The results are demonstration of the capabilities of the current platelet damage accumulation model. It clearly provides invaluable quantitative information regarding flow-induced mechanisms that lead to thrombogenic complications in MHV and other blood-recirculating prosthetic devices.

CONCLUSIONS

A comprehensive CFD simulation of non-Newtonian, transient, and turbulent blood flow past a bileaflet MHV implanted in the aortic position was performed. A complete mapping of the complex flow patterns and the ensuing total stresses was then applied to compute the stress accumulation of platelet flowing along pertinent trajectories within the MHV flow field to quantify their activation potential. Two approaches were employed: first, the activation potential was quantified by integrating the instantaneous stress–exposure time product along the trajectories. Second, the cumulative damage of repeated passages past the valve was computed using a sophisticated damage accumulation model that takes into account the previous loading history of the platelets. To our knowledge, this is the first applica-

tion of such a damage accumulation model to realistic flow conditions found in prosthetic cardiovascular devices. In this initial application of the model, various simplifying assumptions were necessary, still yielding results that predict fairly accurately observed experimental results and clearly demonstrating the predictive capabilities of our model.

In addition to including multiple particle releases representing a large population of platelets, the following enhancements of the damage accumulation model will be employed in the future: each platelet will be assigned random initial damage value to simulate platelets with varying degrees of damage that may be present in the blood. During subsequent passes, this value will be updated by the damage accumulated during the current pass. In the subsequent passes, a different path will be randomly assigned based on a statistical distribution. These model enhancements will facilitate correlations with in vitro measurements of platelet activity that we are currently conducting in prosthetic heart valves in a left ventricular assist device circulation system, and in a computer-controlled hemodynamic shearing device, which is capable of generating prescribed uniform shear stress waveforms extracted from the numerical simulations.

Acknowledgments: This work was supported in part by an Established Investigator Award from the American Heart Association (DB), and by the National Science Foundation under grant no. 0302275 (DB).

REFERENCES

1. Akins CW. Results with mechanical cardiac valvular prostheses. *Ann Thorac Surg* 1995;60:1836–44.
2. Butchart EG, Ionescu A, Payne N, Giddings J, Grunkemeier GL, Fraser AG. A new scoring system to determine thromboembolic risk after heart valve replacement. *Circulation* 2003;108(Suppl 1):II68–74.
3. Bluestein D, Rambod E, Gharib M. Vortex shedding as a mechanism for free emboli formation in mechanical heart valves. *J Biomech Eng* 2000;122:125–34.
4. Sabbah HN, Stein PD. Fluid dynamic stresses in the region of a porcine bioprosthetic valve. *Henry Ford Hosp Med J* 1982;30:134–8.
5. Yoganathan AP, Woo YR, Sung HW. Turbulent shear stress measurements in the vicinity of aortic heart valve prostheses. *J Biomech* 1986;19:433–42.
6. Stein PD, Walburn FJ, Sabbah HN. Turbulent stresses in the region of aortic and pulmonary valves. *J Biomech Eng* 1982;104:238–44.
7. Omoto R, Matsumura M, Asano H, et al. Doppler ultrasound examination of prosthetic function and ventricular blood flow after mitral valve replacement. *Herz* 1986;11:346–50.
8. DeWall RA, Qasim N, Carr L. Evolution of mechanical heart valves. *Ann Thorac Surg* 2000;69:1612–21.
9. Bluestein D. Towards optimization of the thrombogenic potential of blood recirculating cardiovascular devices using modeling approaches. *Expert Rev Med Devices* 2006;3: 267–70.
10. Bluestein D. Research approaches for studying flow induced thromboembolic complications in blood recirculating devices. *Expert Rev Med Devices* 2004;1:65–80.
11. Travis BR, Marzec UM, Leo HL, et al. Bileaflet aortic valve prosthesis pivot geometry influences platelet secretion and anionic phospholipid exposure. *Ann Biomed Eng* 2001;29:657–64.
12. Brown CH, 3rd, Lemuth RF, Hellums JD, Leverett LB, Alfrey CP. Response of human platelets to sheer stress. *Trans Am Soc Artif Intern Organs* 1975;21:35–9.
13. Sutera SP, Mehrjardi MH. Deformation and fragmentation of human red blood cells in turbulent shear flow. *Biophys J* 1975;15:1–10.
14. Brown CH, 3rd, Leverett LB, Lewis CW, Alfrey CP, Jr., Hellums JD. Morphological, biochemical, and functional changes in human platelets subjected to shear stress. *J Lab Clin Med* 1975;86:462–71.
15. Hung TC, Hochmuth RM, Joist JH, Sutera SP. Shear-induced aggregation and lysis of platelets. *Trans Am Soc Artif Intern Organs* 1976;22:285–91.
16. Ramstack JM, Zuckerman L, Mockros LF. Shear-induced activation of platelets. *J Biomech* 1979;12:113–25.
17. Travis BR, Leo HL, Shah PA, Frakes DH, Yoganathan AP. An analysis of turbulent shear stresses in leakage flow through a bileaflet mechanical prostheses. *J Biomech Eng* 2002;124:155–65.
18. Liu JS, Lu PC, Chu SH. Turbulence characteristics downstream of bileaflet aortic valve prostheses. *J Biomech Eng* 2000;122:118–24.
19. Klaus S, Korfer S, Mottaghy K, Reul H, Glasmacher B. In vitro blood damage by high shear flow: human versus porcine blood. *Int J Artif Organs* 2002;25:306–12.
20. Jones SA. A relationship between Reynolds stresses and viscous dissipation: implications to red cell damage. *Ann Biomed Eng* 1995;23:21–8.
21. Shandas R, Kwon J, Valdes-Cruz L. A method for determining the reference effective flow areas for mechanical heart valve prostheses: in vitro validation studies. *Circulation* 2000;101: 1953–9.
22. Leytin V, Allen DJ, Mykhaylov S, et al. Pathologic high shear stress induces apoptosis events in human platelets. *Biochem Biophys Res Commun* 2004;320:303–10.
23. Bluestein D, Li YM, Krukenkamp IB. Free emboli formation in the wake of bi-leaflet mechanical heart valves and the effects of implantation techniques. *J Biomech* 2002;35: 1533–40.
24. Hellums J, Peterson D, Stathopoulos N, Moake J, Giorgio T. Studies on the mechanisms of shear-induced platelet activation. In: Hartman A, Kuschinsky W, eds. *Cerebral Ischemia and Hemorheology*. New York: Springer and Verlag, 1987;80–89.
25. Fogelson AL. Continuum models of platelet-aggregation—formulation and mechanical—properties. *Siam J Appl Math* 1992;52:1089–1110.
26. Tuszynski GP, Rothman VL, Murphy A, Siegler K, Knudsen KA. Thrombospondin promotes platelet aggregation. *Blood* 1988;72:109–15.
27. Merten M, Chow T, Hellums JD, Thiagarajan P. A new role for *P*-selectin in shear-induced platelet aggregation. *Circulation* 2000;102:2045–50.
28. Janes SL, Wilson DJ, Chronos N, Goodall AH. Evaluation of whole blood flow cytometric detection of platelet bound fibrinogen on normal subjects and patients with activated platelets. *Thromb Haemost* 1993;70:659–66.
29. Bevers EM, Comfurius P, Zwaal RF. Mechanisms involved in platelet procoagulant response. *Adv Exp Med Biol* 1993;344: 195–207.
30. Arora D, Behr M, Pasquali M. A tensor-based measure for estimating blood damage. *Artif Organs* 2004;28:1002–15.

31. Pinotti M, Rosa ES. Computational prediction of hemolysis in a centrifugal ventricular assist device. *Artif Organs* 1995;19:267–73.
32. Hellums JD. 1993 Whitaker lecture: biorheology in thrombosis research. *Ann Biomed Eng* 1994;22:445–55.
33. Pinotti M, Rosa ES. Computational prediction of hemolysis in a centrifugal ventricular assist device. *Artif Organs* 1995;19: 267–73.
34. Goubergrits L, Affeld K. Numerical estimation of blood damage in artificial organs. *Artif Organs* 2004;28:499–507.
35. Bludszuweit C. Model for a general mechanical blood damage prediction. *Artif Organs* 1995;19:583–9.
36. Apel J, Paul R, Klaus S, Siess T, Reul H. Assessment of hemolysis related quantities in a microaxial blood pump by computational fluid dynamics. *Artif Organs* 2001;25: 341–7.
37. Bluestein M, Mockros LF. Hemolytic effects of energy dissipation in flowing blood. *Med Biol Eng* 1969;7:1–16.
38. Yeleswarapu KK, Antaki JF, Kameneva MV, Rajagopal KR. A mathematical model for shear-induced hemolysis. *Artif Organs* 1995;19:576–82.
39. Grigioni M, Morbiducci U, D'Avenio G, Di Benedetto G, Del Gaudio C. A novel formulation for blood trauma prediction by a modified power-law mathematical model. *Biomech Model Mechanobiol* 2005;4:249–60.
40. King MJ, David T, Fisher J. Three-dimensional study of the effect of two leaflet opening angles on the time-dependent flow through a bileaflet mechanical heart valve. *Med Eng Phys* 1997;19:235–41.
41. Kelly SG, Verdonck PR, Vierendeels JA, Riemslagh K, Dick E, Van Nooten GG. A three-dimensional analysis of flow in the pivot regions of an ATS bileaflet valve. *Int J Artif Organs* 1999;22:754–63.
42. Krafczyk M, Cerrolaza M, Schulz M, Rank E. Analysis of 3D transient blood flow passing through an artificial aortic valve by Lattice–Boltzmann methods. *J Biomech* 1998;31:453–62.
43. Grigioni M, Daniele C, Del Gaudio C, et al. Three-dimensional numeric simulation of flow through an aortic bileaflet valve in a realistic model of aortic root. *ASAIO J* 2005;51:176–83.
44. Bluestein D, Niu L, Schoephoerster RT, Dewanjee MK. Fluid mechanics of arterial stenosis: relationship to the development of mural thrombus. *Ann Biomed Eng* 1997;25:344–56.
45. Kiris C, Kwak D, Rogers S, Chang ID. Computational approach for probing the flow through artificial heart devices. *J Biomech Eng* 1997;119:452–60.
46. Wilcox DC. Simulation of transition with a two-equation turbulence model. *AIAA J* 1994;32:247–55.
47. Yin W, Alemu Y, Affeld K, Jesty J, Bluestein D. Flow-induced platelet activation in bileaflet and monoleaflet mechanical heart valves. *Ann Biomed Eng* 2004;32:1058–66.
48. Yin W, Gallocher S, Pinchuk L, Schoephoerster RT, Jesty J, Bluestein D. Flow induced platelet activation in a St. Jude MHV, a trileaflet polymeric heart valve and a St. Jude tissue valve. *Artif Organs* 2005;29:826–31.
49. Ge L, Jones SC, Sotiropoulos F, Healy TM, Yoganathan AP. Numerical simulation of flow in mechanical heart valves: grid resolution and the assumption of flow symmetry. *J Biomech Eng* 2003;125:709–18.
50. Ge L, Leo HL, Sotiropoulos F, Yoganathan AP. Flow in a mechanical bileaflet heart valve at laminar and near-peak systole flow rates: CFD simulations and experiments. *J Biomech Eng* 2005;127:782–97.
51. Edmunds LH, Norwood WI, Low DW. *Atlas of Cardiothoracic Surgery*. Philadelphia, PA: Lea and Febiger, 1990.
52. Chaux A, Blanche C. Technical aspects of valvular replacement with the St. Jude prosthesis. *J Cardiovasc Surg (Torino)* 1987;28:363–8.
53. Bluestein D, Einav S. Transition to turbulence in pulsatile flow through heart valves—a modified stability approach. *J Biomech Eng* 1994;116:477–87.
54. Bluestein D, Einav S. Techniques in the analysis of stability of pulsatile flow through heart valves. In: Leondes CT, ed. *Biomechanics Systems Techniques and Applications: Cardiovascular Techniques*, Vol. II. Boca Raton, FL: CRC Press LLC, 2001;4-1–4-39.
55. Gosman A, Ioannides L. Aspects of computer simulation of liquid-fuelled combustors. *AIAA J Energy* 1983;7:482–90.
56. Merrill EW, Gilliland ER, Cokelet G, Shin H, Britten A, Wells RE, Jr. Rheology of human blood, near and at zero flow. Effects of temperature and hematocrit level. *Biophys J* 1963;3:199–213.
57. Schulz-Heik K, Ramachandran J, Bluestein D, Jesty J. The extent of platelet activation under shear depends on platelet count: differential expression of anionic phospholipid and factor Va. *Pathophysiol Haemost Thromb* 2005;34:255–62.
58. Leverett LB, et al. Red blood cell damage by shear stress. *Biophys J* 1972;12:257–73.
59. Wurzinger LJ, Blasberg P, Schmid-Schonbein H. Towards a concept of thrombosis in accelerated flow: rheology, fluid dynamics, and biochemistry. *Biorheology* 1985;22:437–50.
60. Grigioni M, Daniele C, Morbiducci U, D'Avenio G, Di Benedetto G, Barbaro V. The power-law mathematical model for blood damage prediction: analytical developments and physical inconsistencies. *Artif Organs* 2004;28:467–75.